Microstructural defects in nanocrystalline iron probed by x-ray-absorption spectroscopy

Andrea Di Cicco, Mario Berrettoni, and Sergio Stizza

*Dipartimento di Matematica e Fisica, Università degli Studi di Camerino,
Via Madonna delle Carceri, I-62032 Camerino (MC), Italy*

Ennio Bonetti

Dipartimento di Fisica, Università degli Studi di Bologna, Viale Berti Pichat 6/2, I-40126 Bologna, Italy

Giorgio Cocco

Dipartimento di Chimica, Università di Sassari, Via Vienna 2, I-07100 Sassari, Italy

An EXAFS (extended x-ray-absorption fine structure) study of nanocrystalline iron prepared by high-energy ball milling is presented. Accurate data analysis has been performed using a recently developed *ab initio* multiple-scattering method (GNXAS). The crystalline iron EXAFS spectrum, taken as reference, has been analyzed taking proper account of the important multiple-scattering signal. Results of the data analysis are shown to be in good agreement with known structural values. The dramatic decrease of the first-neighbor coordination number found in nanocrystalline iron, as a function of the milling time, is shown to be related to the presence of a large defect density. The corresponding decrease of the coordination numbers of the second and further neighbors, as well as the significant decrease of the multiplicities of the three-atom configurations, confirms this interpretation. A simple model which takes into account the presence of atomic defects is shown to lead to marked reduction of coordination numbers and three-atom multiplicities in agreement with the experimental data. Selected models without lattice defects are shown to be unable to give a quantitative explanation of the intensity reduction of the EXAFS signal found in milled nanocrystalline iron. An *in-situ* annealing of the sample (up to about 1100 ° C) milled for the longer time (32 h) is shown to reduce considerably the density of the defects, as expected, although no complete recovering of the crystalline order is found. The transition from α iron to γ iron has been directly observed for such nanocrystalline material.

I. INTRODUCTION

Nanocrystalline metals and alloys are a relatively new class of materials which attracted interest in recent times due to their peculiar physical and chemical properties. This field of research has a strong impact on several disciplines ranging from chemistry of catalysts, material science, and basic physics.[1]

There are several methods to produce nanocrystalline materials with sizes in the range 5–1000 Å. Without regard of the methods of preparation of clusters, one of the most important basic properties to be studied is certainly the atomic structure. Better knowledge of the microscopic structure can help in understanding several related microscopic and macroscopic characteristics of such systems. Usually, structural characterization and study of shape and morphology are carried out by standard means such as x-ray diffraction and electron microscopy.[2] However, a technique sensitive to short-range order is required for detailed structural investigations, especially for nanocrystallites of small dimensions.

X-ray-absorption spectroscopy (XAS) is certainly a suitable technique for structural studies of such systems which do not present long-range order.[3] The XAS technique is sensitive to the local structure up to 5–10 Å

around photoabsorbing sites, selected by their atomic number. The local two-atom distribution $g_2(r)$ can be determined with good accuracy and quantitative information on the three-atom distribution $g_3(r_1, r_2, \theta)$ can be derived indeed.[4,5] The sensitivity of XAS to the three-atom distribution is due to the strong effective interaction between the local probe (the photoelectron) and surrounding matter.

The capability of XAS to probe three-atom correlations is unique and makes the application of this spectroscopy to systems without long-range order particularly interesting. Quite recently, quantitative information about local two-atom and three-atom distribution functions in amorphous[6] and liquid systems[7] has been obtained by using an original scheme[4,5] employing *ab initio* calculations of the absorption cross section in the framework of the multiple-scattering (MS) theory (Ref. 8 and references therein). The technique has been successfully used in the case of gas-phase molecules[9,10] and complex crystalline systems such as perovskites[11] giving information about the bond-angle distribution.

In this paper we present an application of such *ab initio* data analysis to EXAFS (extended x-ray-absorption fine structure) spectra of nanocrystalline iron prepared by high-energy ball milling.[12] This mechanical procedure

    <u>50</u>   12 386

allows one to obtain iron crystallites with grain sizes of the order of nanometers. We have analyzed Fe powders obtained after different milling times which show different average grain sizes in the range 70–200 Å.[13]

XAS has been used quite often for investigating the local structure of nanocrystalline materials and/or clusters produced using different techniques. Generally, a marked reduction of the first-neighbor coordination number (CN) has been observed for nanocrystallites of sizes in the same range of those of the present work (see for example Refs. 14–16). For smaller cluster sizes variations of the average interatomic distances R and of the mean-square relative displacements σ_R^2 have been observed (see for example Ref. 17). The existence of anharmonic vibrations, leading to non-Gaussian shapes of the first peak of the pair distribution function, has been also pointed out.[18] Up to now, the study of EXAFS data of nanocrystalline materials has been usually carried out using standard methods for data analysis including only the first-neighbor single-scattering contribution. In this work we have performed a quantitative analysis of Fe K-edge EXAFS spectra by using ab initio MS codes for data analysis (GNXAS).[4,5]

The paper is organized as follows: In Sec. II experimental details concerning the preparation and execution of EXAFS measurements are described; in Sec. III the results of the data analysis of the bulk model and nanocrystalline iron, as well as the methods used in the application of ab initio calculation procedures, are reported; in Sec. IV the main conclusions of this work are given.

II. EXPERIMENTAL DETAILS

Pure iron powders (325 mesh, Alfa products, 99.9% purity) were milled for selected times at room temperature in a hardened tool steel vial with a SPEX mixer mill (model 8000). In order to minimize contaminations all the milling treatments were performed under an argon atmosphere (oxygen content below 5 ppm). The weight of the mixed powders was about 10 g and the ball-to-powder ratio was 8/1. After different milling times the mechanical attrition was interrupted and a small quantity of the milled powders was removed for the subsequent characterization.

The average grain size $\langle D \rangle$ and the average microstrain were evaluated by x-ray diffraction (XRD).[13,19] The microstructural evolution of the milled powders as a function of the milling times has been found to be similar to that previously observed in iron and other pure metals.[13,20–24] In particular, a progressive size reduction, up to 90% of the ultimate value, is experienced in short times, approximately 10–20 h milling in our experimental conditions, as indicated by the mean crystallite sizes $\langle D \rangle$ reported in Table I. Prolonged milling up to 40 h resulted in a further grain size reduction up to the ulti-

mate value of 80 Å, in agreement with the value reported by Fecht et al. of 90 Å.[20] No further appreciable refinement could be observed after extending milling times. Moreover, whereas at shorter milling times a greater scattering in the grain dimensions has been observed, this is strongly reduced at the ultimate grain size and is of the order of 20%. The grain size refinement is accompanied in the early milling stages by a strong microstrain increase that saturates at approximately 10–20 h milling.[21] Transmission electron microscopy (TEM) observations gave evidence of nearly spherical shaped grains when reaching the ultimate grain size, in agreement with previous results obtained by ball milling in similar experimental conditions.[13,20]

Samples of iron powders suitable for XAS spectroscopy, hereafter called 2 h, 8 h, 16 h, and 32 h according to the milling time, have been prepared and tested in advance, taking care of the severe requirements of thickness and homogeneity needed to perform accurate absorption measurements. Finely ground powder of milled Fe powders, preserved in a dry box to avoid possible chemical reactions, was dispersed in water-free ethanol. The suspension was left at rest for some time to allow precipitation of the largest particles. Average particle size in the suspension was in the micrometric range. The suspension was then filtered using a Millipore polycarbonate membrane. In this way, a rather uniform layer of powders has been obtained.

Thicknesses of the samples were chosen in order to obtain the best signal-to-noise ratio in absorption measurements (jump of the absorption coefficient of about 1). Optimization of samples and preliminary measurements have been performed at the University of Camerino using the EXAFS laboratory equipment (Centro Interdipartimentale Grandi Apparecchiature).

X-ray-absorption measurements of milled iron at the Fe K edge ($\approx$ 7120 eV) have been performed at LURE (Laboratoire pour L'Utilisation du Rayonnement Electromagnètique) on the D-42 and D-44 beam lines [equipped with Si (331) channel-cut and Si (311) monochromators, respectively] by using synchrotron radiation emitted by the storage ring DCI working at 1.85 GeV with typical currents of 300 mA. A reference spectrum of crystalline iron has been also measured using a commercial 10 μm foil (Goodfellow). Samples have been measured in transmission mode at room temperature. Measurements show a very high signal-to-noise ratio and cover a wide range of wave-vector values (0–16 Å^{-1}).

The 32 h powder has been also measured at higher temperatures, up to 1100 °C, by using a special furnace working in vacuum.[25] In this case the sample was a dispersion of milled Fe powder into a boron nitride (BN) matrix. This original preparation technique has been proved to be successful for high-quality measurements at high temperatures.[25,26]

III. AB INITIO EXAFS ANALYSIS: RESULTS AND DISCUSSION

In this section we present the experimental results of our x-ray-absorption study of nanocrystalline milled Fe

TABLE I. Average grain size $\langle D \rangle$ as a function of milling time as obtained by XRD data Ref. (13).

Milling time (h)	2	8	16	32
$\langle D \rangle$ (Å)	250	100	90	80

powders, taking as reference the bulk iron spectrum. For sake of clarity, this section is divided into several subsections which tackle different issues of the EXAFS data analysis performed using *ab initio* MS signals. We first present raw experimental data and Fourier transform in order to discuss the qualitative features of the spectra. Section III B is devoted to the presentation of the results of the MS data analysis for crystalline iron which serves as a model. Section III C is focused on the specific problem of the reduction of coordination numbers and multiplicities of triangular configurations for crystallites in the nanometric range. Results of the MS data analysis of nanocrystallites are presented in Sec. III D. A XAS study of the 32 h milled sample at high temperatures is presented in Sec. III E.

A. Qualitative discussion of EXAFS spectra

In Fig. 1 we show Fe K-edge $k^2\chi(k)$ EXAFS spectra of the 2 h, 8 h, 16 h, and 32 h milled nanocrystalline iron. Fourier transform (FT) spectra performed in the range 2.8–15 Å^{-1} are shown in Fig. 2. The spectra are compared with the pure crystalline iron one, recorded in the same run. It is clear that the bcc local structure is preserved. As has been previously observed in other nanocrystalline materials, there is clear evidence for a reduction of the first-neighbor coordination number (and consequently of the coordination number of the farther shells). The area of the first peak of the FT's, located at about 2.1 Å due to the effect of the phase shifts, is reduced up to about 50% (16 h and 32 h cases).

Of course, the strong reduction of the first-shell coordination number cannot be explained by the estimated sizes of the nanocrystallites, if one assumes that crystallites have spherical shape with an ideal crystalline structure. As shown in the next sections, the reduction due to the surface effect should be limited to a few percent
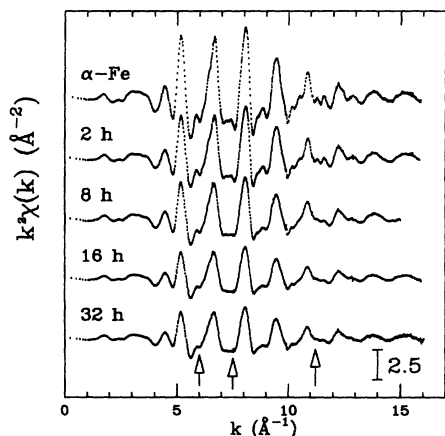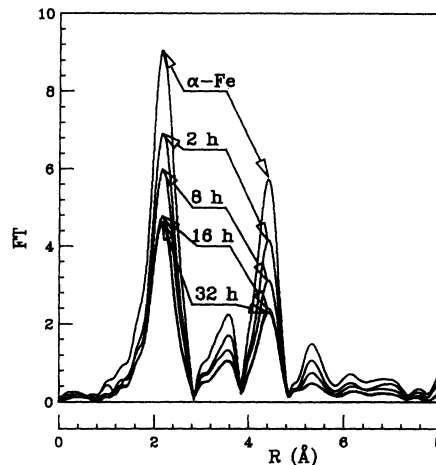

FIG. 2. Fourier transform (FT) of the EXAFS $k^2\chi(k)$ spectra (reported in Fig. 1) of bulk iron and nanocrystalline samples.

for first neighbors. Disorder of first-neighbor distances, as we shall see, is not able to account for such a reduction of the first peak of the two-atom distribution $g_2(r)$. The lack of coordination indicates the existence of a large fraction of Fe sites where CN's are much less than 8 (bulk value). On the other hand, some kind of chemical bonding must exist both in the crystallites and in the grain boundaries. In this way one is led naturally to consider the existence of defects in the structure, which can have a different nature but always conduct to a reduction of the coordination numbers. The increasing importance of the defects as a function of milling time is also recognized by x-ray-diffraction analysis.[22–24] In fact, studies of the broadening of the Bragg peaks in nanocrystallites show increasing values of the root-mean-square strain, a quantity related to the density of defects both in the grains and in the grain boundaries.[24,19]

A deeper analysis of EXAFS spectra is certainly needed to obtain quantitative results on the local structure of these iron nanocrystallites. As we shall see, EXAFS spectra contain a lot of contributions due to two-atom and three-atom configurations confined within a few Å. The reduction of amplitude of the $\chi(k)$ signals observed in nanocrystalline materials depends naturally on the interatomic distances involved. For example, it is interesting to note that there is a more pronounced reduction of the FT peaks (Fig. 2) located at higher distance values, which are due to farther atoms and to triangular configurations involving mainly first and second neighbors. The stronger damping of the high-frequency components can be easily seen in the EXAFS spectra of Fig. 1: The high-frequency components giving rise, for example, to the features indicated by the arrows in Fig. 1 are progressively quenched in the Fe milled samples.

Therefore, quantitative analysis of the high-frequency features can give useful information about the local atomic arrangement in such materials. In the successive subsections we present results of a data analysis of nanocrystalline iron performed using the multiple-scattering theory.[4,5]

FIG. 1. Experimental Fe K-edge EXAFS $k^2\chi(k)$ spectra (a) of iron powders prepared by high-energy ball milling at different milling times (2 h, 8 h, 16 h, and 32 h) compared with the bulk iron spectrum. In the lower panel (b) the Fourier transform of the EXAFS spectra is shown.

B. Methodology: crystalline iron EXAFS analysis

The Fe K-edge EXAFS spectrum of crystalline iron has been analyzed by using the GNXAS package of programs.[4,5] The programs provide an *ab initio* multiple-scattering calculation of the absorption cross section which is used to fit the raw experimental data. This approach[5,27] has been tested and used for analyzing several systems ranging from gas-phase molecules,[9,10] metal[7] and molecular[28] liquids, crystalline systems,[11] and biological matter.[29] Here we briefly recall the main features of the method.

The absorption cross section σ can be written as a product of an atomic cross section σ_0, which is smooth as a function of energy, and a structural term $[1+\chi(k)]$ which oscillates as a function of the wave vector $k = \sqrt{E - E_0}$ (E_0 is the threshold energy). The central step in the calculation of the structural term $\chi(k)$, in the framework of the MS theory within the muffin-tin approximation,[8] is the inversion of a matrix $(I + GT)$ containing phase shifts (matrix T) and propagators (matrix G) which describe the final state photoelectron in a selected cluster of atoms (see for example Ref. 30 and references therein). The cluster size useful for such calculation (10–20 Å) is mainly limited by the short lifetime of the excited state and by the shape of the G matrix.

The total inversion of the $(I+GT)$ matrix can be easily performed only at low energies, say, within 50–80 eV beyond the threshold, because of the low number of angular momenta needed in the calculation. Moreover, there are serious difficulties in performing thermal and configurational averages of the calculated cross sections.

A power series expansion of the $(I + GT)^{-1}$ matrix is usually convergent in the high-energy limit and the first nontrivial term, representing the single-scattering (see for example Ref. 31 and references therein), has been widely used to analyze EXAFS spectra.[3] Each term of the expansion represents a signal associated with a particular MS pathway. The structural term of the absorption cross section can be written as a sum of multiple-scattering signals which oscillate as a function of energy. The single-scattering term contributing to the structural signal is usually called χ_2. However, convergence can be very slow and important multiple-scattering effects are usually found in the high-energy regime too, particularly in crystalline structures (see for example Refs. 32, 11 and references therein). There are practical difficulties in applying the multiple-scattering series expansion mainly because of the great number of contributions (MS pathways) to be considered to achieve convergence.

A different approach consists in calculating directly the total contribution to the cross section due to couples, triplets, and quadruplets of atoms. Calculation of the total signals due to a few atoms is very fast also at high energies by using the continued-fraction algorithm.[30] Proper n-body signals $\gamma^{(n)}$ are defined by subtracting low-order terms from n-atom total calculations.[27] The $\gamma^{(n)}$ n-body signal due to a particular configuration of n atoms, in the region of convergence of the MS series, is equal to the sum of the χ_m terms ($m \geq n$) associated with the same atomic configuration. The convergence of the series of the n-body signals $\gamma^{(n)}$ is never worse than the convergence of the power series expansion (χ_m). In particular, it has been often found that four-body contributions can be generally neglected (while in the power series χ_4 signals associated with two-atom and three-atom configurations are often very important).

The structural term associated with a cluster of $n + 1$ atoms can then be written as

$$\chi(0, 1, 2, ..., n) = \sum_i \gamma^{(2)}(0, i) + \sum_{(i,j;j>i)} \gamma^{(3)}(0, i, j)$$
$$+ \sum_{(i,j,k;j>i,k>j)} \gamma^{(4)}(0, i, j, k) + \cdots$$
$$+ \gamma^{(n)}(0, 1, 2, ..., n), \qquad (1)$$

where usually only the first two terms have to be taken into account. In this way, by using Eq. (1), it is possible to establish quite simple relationships between structure and signals in terms of the main two-atom and three-atom configurations.

Another important aspect of the theory is how the thermal (configurational) average of the signals has to be done. An appropriate theory has to be applied for calculating the averages of the n-body signals.[33,27] The signals (χ_m or γ) to be averaged are oscillating functions of the type

$$f(k) = A(k, R) \sin[kR_p + \phi(k, R)], \qquad (2)$$

where $A(k, R)$ and $\psi = (kR_p + \phi)$ are smooth functions of k and of the geometrical parameters R. The main frequency of the signal is, in the case of a χ_m term of the power expansion, the path length R_p. However, as the $\gamma^{(n)}$ signals are sums of χ_m signals one obtains that the γ functions are again oscillating signals with a dominant frequency equal to the path length of the shortest (i.e., lowest-order) paths of the corresponding MS series.

The configurational average of the signals is given by

$$\langle \chi(k) \rangle = \mathrm{Im} \int dr A(k, r) \exp[i\psi(k, r)] P(r), \qquad (3)$$

where $P(r)$ is the normalized distribution function centered at the mean R coordinates of the n-atom configuration under consideration. If the $P(r)$ distribution is sufficiently narrow, a Taylor expansion of amplitude $A(k, r)$ and phase $\psi(k, r)$ functions can be safely used to evaluate the integral (3). Derivative of amplitude and phase functions with respect to the geometrical coordinates can be calculated numerically. Simple analytical expressions taking properly into account configurational averages and variation of mean coordinates can be derived by using a Gaussian distribution function $P(r)$ [for a two-atom configuration we have $P(r) = 4\pi r^2 \rho g_2(r)$].[33] In this case, $P(r)$ is defined by variances and correlations of the coordinates (covariance matrix). For example, for a two-atom configuration (defined by the distance R) one has only σ_R^2 while for a three-atom configuration (defined by two distances R_1, R_2 and one angle θ) the three variances σ_{R1}^2, σ_{R2}^2, σ_θ^2 and correlations $\sigma_{R1,R2}^2$, $\sigma_{R1,\theta}^2$, $\sigma_{R2,\theta}^2$ have to be considered.

For non-Gaussian peaks of the two-atom and three-

atom distributions it is possible to use the cumulant expansion and again general analytical expression have been derived.[33] However, the cumulant expansion converges rapidly only for slight corrections to the Gaussian shape and in the case of broad distributions other methods should be devised.[27]

The GNXAS programs provide a fit of the raw experimental data incorporating all the above-mentioned algorithms developed to calculate configurational averages of the $\gamma^{(n)}$ signals. Calculation of the $\gamma^{(n)}$ functions is performed by using a muffin-tin potential and advanced models for the energy-dependent exchange-correlation self-energy. A cluster analysis is performed and the χ or γ multiple-scattering signals are classified according to the geometrical coordinates of the relevant n-body configurations. The final fit of the experimental data is performed directly on the raw data (without Fourier filtering) using a standard square residual function which allows statistical analysis of the results.

In order to perform such an *ab initio* data analysis in the case of crystalline iron, it is necessary to identify the two-atom and three-atom configurations present in the bcc structure. The main frequency content of the EXAFS signal is confined within 5 Å (see Fig. 2). The two-atom and three-atom configurations having a half-perimeter length $(R_p/2)$ within this cutoff value are reported in Table II and classified according to their length. In Table II, the n-atom configurations are classified as isolated "peaks" of the n-body distribution functions g_n. While two-atom configurations are defined by a single mean distance R, the triangular configurations are defined by the two shortest distances R_1 and R_2 and the angle in between θ. The multiplicity N represents the number of triangular configurations per atom. A pictorial view of the two-atom and three-atom configurations relevant to the bcc structure is contained in Ref. 34, Fig. 2.

The γ signals associated with two-atom and three-atom configurations have been calculated by using nonoverlapping muffin-tin potentials and a Hedin-Lundqvist complex and energy-dependent self-energy. Muffin-tin radii $R_{MT} \approx 0.87$ Å (corresponding to about 23 of integrated electron charge density) have been used. Both the continued-fraction algorithm and the power expansion have been used to calculate n-body signals which

were found to be identical using the two methods of calculation.

The proper n-body γ signals of both the first five shells and of the first four three-atom configurations have been used to fit the experimental spectra of crystalline iron. Structural parameters were only the cell side and the independent variances (of distances and angles) and possible correlation parameters of the covariance matrices.[35]

In particular, only the first-neighbor bond variance σ_{R1}^2, the fourth-shell one σ_{R4}^2, and four angle variances associated with the triangular configurations were used. The other distance variances can be easily calculated due to the geometrical constraints. The bond-bond ρ_{RR} and bond-angle correlations $\rho_{R\theta}$ have been confined in a narrow range of values around zero. However, the EXAFS spectrum has been found to show a low sensitivity to these parameters, apart from the first-neighbor bond-bond correlations (ρ_{R1R1}).

In Fig. 3, calculated best-fit MS signals and experimental EXAFS $\chi(k)$ of bulk iron are reported as a function of the wave vector k. Curves are presented multiplied by k^2. As mentioned above, the fitting procedure has been performed directly using the experimental x-ray-absorption coefficient (proportional to the cross section σ) written as

$$\alpha(E) = \alpha_0(E)[1 + \chi(E)] + \alpha_{bkg}(E) + \alpha_{exc}(E), \quad (4)$$

where $\alpha_0(E)$ is the one-electron atomic absorption, mod-

TABLE II. Two-atom (g_2) and three-atom (g_3) configurations in the bcc structure. Distances are normalized to the cell parameter a; the angle θ is measured in degrees.

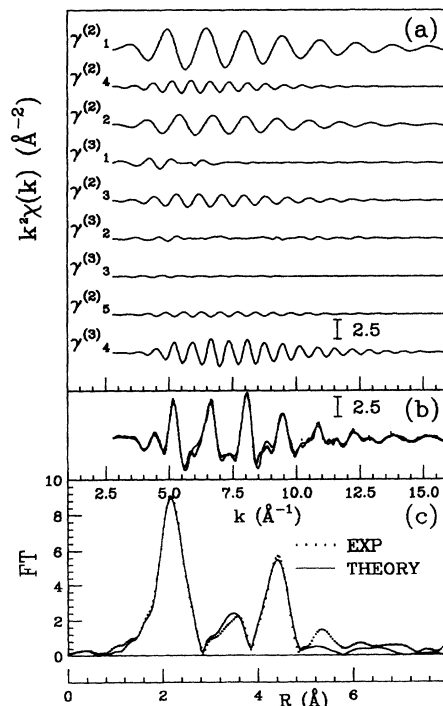|	R_1/a	R_2/a	θ (deg)	N	R_3/a
$g_2^{(1)}$	$\sqrt{3}/2$			8	
$g_2^{(2)}$	1			6	
$g_2^{(3)}$	$\sqrt{2}$			12	
$g_2^{(4)}$	$\sqrt{11}/2$			24	
$g_2^{(5)}$	$\sqrt{3}$			8	
$g_3^{(1)}$	$\sqrt{3}/2$	$\sqrt{3}/2$	70.53	12	1
$g_3^{(2)}$	$\sqrt{3}/2$	$\sqrt{3}/2$	109.47	12	$\sqrt{2}$
$g_3^{(3)}$	1	1	90	12	$\sqrt{2}$
$g_3^{(4)}$	$\sqrt{3}/2$	$\sqrt{3}/2$	180	4	$\sqrt{3}$

FIG. 3. Proper two-atom and three-atom multiple-scattering contributions to EXAFS of crystalline iron (a). Comparison between calculated (solid line) and experimental (dotted line) crystalline iron $k^2\chi(k)$ (b). Fourier transform (FT) of experimental (dotted line) and calculated (solid line) signals.

eled as hydrogenic, $\alpha_{\rm bkg}$ is a smooth polynomial background, and $\alpha_{\rm exc}$ represents the contribution of possible many-electron channels.

In the upper panel (a) of Fig. 3 the proper two-atom and three-atom signals are shown from the top to the bottom. The first two MS signals $\gamma_1^{(2)}$ and $\gamma_4^{(2)}$ are the proper two-atom signals associated with the first and the fourth shell of neighbors, respectively. The third and fourth γ signal are related to the first triangular configuration distribution ($g_2^{(2)}$ and $g_3^{(1)}$). The $\gamma_2^{(2)}$ signal is the proper two-atom signal related to second neighbors while the $\gamma_1^{(3)}$ represents the proper three-atom signal. The successive two γ signals are associated with the second three-body configuration ($g_2^{(3)}$ and $g_3^{(2)}$). The seventh γ signals is the proper three-atom contribution due the third triangular configuration of Table II ($g_3^{(3)}$). The last two curves are related to the collinear configurations involving first and fifth neighbors. As expected, the proper three-atom contribution ($\gamma_4^{(3)}$) is much stronger than the fifth-shell two-atom one ($\gamma_5^{(2)}$) due to the well-known focusing effect. This occurrence was already pointed out by using earlier plane-wave theories[36] applied to the iron case.[37] Here we remark only that the thermal average of the MS terms[33] arising from collinear configurations needs an appropriate theory to be applied.[39,27]

In the center panel (b) the total best-fit MS signal and the experimental structural term $k^2\chi(k)$ are shown. The agreement is excellent in the whole energy range and the unexplained features are mainly due to contributions located in the region above 5 Å in R space. This is clearly seen in the FT spectra reported in Fig. 3, lower panel (c), where a very good agreement between calculated and experimental spectra is found for $R < 5$ Å.

The best-fit structural parameters and their estimated statistical errors (in brackets), accounting for correlation among parameters, are reported in Table III. As anticipated, the actual structural parameters used to average the second-, third-, and fourth-neighbors contributions were the angular variance and the bond-bond and bond-angle correlations. In this way the same parameters are employed to average both the three-atom and the two-atom contributions. Angular standard deviations σ_θ were found to be around 1.8° for the first three triangular configurations and around 0.8° for the fourth (collinear) configurations. The bond-bond correlation of the collinear configuration (see Table III) $\rho_{R1R1}^{(4)}$ was found to be neg-

ative, indicating a slight anticorrelation of these first-neighbor bonds, while the other correlations were found not to affect appreciably the total signal and have been found to be $\rho_{RR} = \rho_{R\theta} = 0.0$ (3). In Table III the best-fit structural parameters (first row) are compared with results obtained by using diffraction techniques. The slight shortening of the cell side a obtained by using this ab $initio$ EXAFS analysis can be mainly attributed to systematic errors in the theoretical calculation. The statistical error is found to be very low as indicated in Table III. The $\sigma_{\rm I}^2$ bond variance is in nice agreement with previous calculations based on the phonon density of states measured using neutron diffraction (row 3; see Ref. 38). The second-shell atoms are instead found to be slightly more correlated as indicated by the lower value of $\sigma_{\rm II}^2$. The distance variance of the successive shells of neighbors is found to approach the limiting value for the distance variances $2\langle u^2\rangle$, valid for uncorrelated atoms. The high statistical error on the $\sigma_{\rm IV}^2$ value is due to the relative weak intensity of the signal. Possible deviations from the Gaussian approximation have been investigated by using the cumulant expansion. We obtained very small values for the asymmetry parameter $\beta = K_3/\sigma_{R1}^3$ for the first-neighbor distribution, indicating that the harmonic approximation holds at room temperature ($\beta = 0.1\pm0.1$).

The nonstructural parameters used in the fitting procedure were the threshold energy E_0 to be added to the theoretical energy scale (continuum threshold) and the S_0^2 factor taking into account the reduction of amplitude due to different excitation channels. The E_0 energy was found to coincide within 0.5 eV with the energy position of the second peak of the derivative (around 7120 eV) of the experimental spectrum, which has been also used to calculate the k scale of the figures. The S_0^2 factor has been found to be around 0.85 in good agreement with theoretical estimates.[40] The finite energy resolution of the monochromator affecting the experimental spectrum has been taken into account by introducing a Gaussian-shaped function with standard deviation of about 0.5 eV. As usual, the $\alpha_{\rm bkg}(E)$ term in Eq. (4) has been modeled as a smooth polynomial spline. A step-shaped $\alpha_{\rm exc}(E)$ contribution[9,41] has been used to account for the opening of the double-electron [1s3s] channel. The inclusion of double-electron excitation channels has been recently found necessary for reliable studies of EXAFS spectra.[9,41–43] The energy onset has been found to be 95 ± 5 eV, in agreement with the $Z + 1$ approximation,

TABLE III. Results of the present EXAFS data analysis of crystalline iron compared with the cell parameter a derived from x-ray diffraction (XRD) and with calculated mean-square vibrational amplitudes based on neutron-diffraction measurements of the phonon density of states. Mean-square vibrational amplitude ($\langle u^2\rangle$) and distance variances (σ^2) are presented in units of 10^{-3} Å^2.

	a (Å)	$2\langle u^2\rangle$	$\sigma_{\rm I}^2$	$\sigma_{\rm II}^2$	$\sigma_{\rm III}^2$	$\sigma_{\rm IV}^2$	$\sigma_{\rm V}^2$	$\rho_{R1R1}^{(4)}$
EXAFS	2.855 (5)		4.7 (6)	5.7 (7)	7.8 (8)	11 (2)	7.5 (8)	-0.2 (1)
XRD (293 K)	2.8662 (5)[a]							
Theory		9.0[b,c]	5.06[b]	6.6[b]				

[a]Reference 45.

[b]Reference 38.

[c]Reference 46.

and the relative weight was found to be $3\pm1\%$ of the main $1s$ edge.

The very successful *ab initio* MS data analysis of the K-edge EXAFS spectrum of crystalline iron provides us with a reliable tool to investigate the related structure of our nanocrystalline iron samples. The background model and the nonstructural parameters have been kept fixed in the EXAFS data analysis presented in Sec. III D in order to compare local structural characteristics of nanocrystalline and bulk iron. The main changes, as we shall see, concern the multiplicities of the two-atom and three-atom configurations. The next subsection is devoted to the specific problem of possible reductions of local coordination.

C. Loss of local coordination in nanocrystalline iron

Coordination numbers and multiplicities of three-atom configurations tend to decrease according to the size of the crystallites. Of course, this is due to the existence of surface atoms which cannot be fully coordinated. In Fig. 4 the calculated multiplicities of the main two-atom and three-atom configurations present in the bcc local structure are reported as a function of cluster size. The simulated cluster has been obtained by imposing a distance cutoff length and has an approximate spherical shape with a perfect crystalline structure. As shown in Fig. 4, for a cluster size in the range 70–100 Å a 5% reduction of the first-neighbor CN is obtained. Multiplicities of the triangular configurations are more strongly damped although with percentages not exceeding 10%. In this size range, the particular shape of the cluster does not influence appreciably the final result on the coordination numbers, due to the large volume-to-surface ratio.
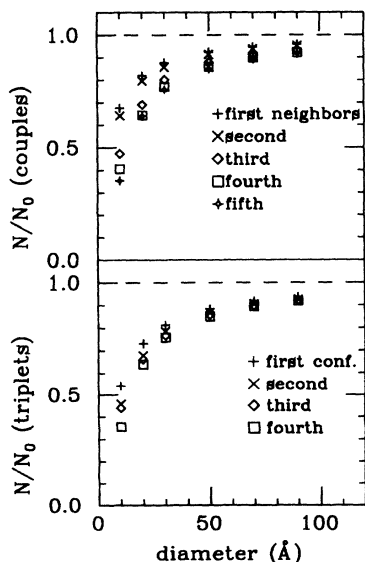

FIG. 4. Multiplicities of two-atom (upper panel) and three-atom (lower panel) configurations as a function of the cluster size (diameter). Perfect bcc structures have been used (see text). Multiplicities have been normalized to the ideal crystal case (N_0).

The simple model of a sample composed of separated clusters of 70–200 Å is clearly not able to explain the experimental spectra of Fig. 1. As a matter of fact, a single powder grain of the milled material (of micrometric size) is known to be composed of nanometer-sized clusters, possibly identified by coherently diffracting domains, having large-angle grain boundaries. The density of such materials can range between 0.5 and 1 with respect to that of the bulk crystalline counterpart. The excess free volume has been mainly attributed to the grain boundaries, where atomic density is supposed to be very low. From a *local* point of view, however, there must be at least a partial coordination of the Fe atoms, i.e., chemical bonding, ensuring connectivity to the structure. In presence of an instability of the grain boundaries, the two-body distribution function $g_2(r)$ should anyway resemble that of a liquid or glassy metal, which shows a well-defined first-neighbor distance. In the absence of the first peak of the $g_2(r)$, the atoms would be free to move as they do in the vapor state. However, a model with a structureless $g_2(r)$ in the grain-boundary region was proposed a few years ago in order to explain both diffraction[44] and EXAFS spectra[14] of nanocrystalline materials. Thus, the lack of coordination has been indicated to be due to the fraction of atoms belonging to the grain boundaries which would show neither short-range nor long-range order.

Another approach that can be used to explain EXAFS and diffraction results is to take into account the existence of microstructural defects such as dislocations, twins, and atomic and multiatomic (voids) vacancies. The inclusion of defects in the structure would artificially increase the number of "surface," ill-coordinated, atoms. The strain measured by x-ray diffraction, for example, is an indirect measure of the density of structural defects. Other important thermodynamic quantities (such as specific heat, for example) are related to lattice defects. As anticipated, there is evidence of increasing large strains as a function of milling time.[22–24] Therefore, there is large evidence that a not-negligible density of defects exists in the structure of nanocrystallites, especially in mechanically produced nanocrystalline materials.

Our problem is to determine whether the introduction of lattice defects could lead to a reduction of the first-neighbor coordination number of the same order of magnitude of those observed by EXAFS. At the same time, a model taking into account defects could also serve as a basis to estimate CN's and multiplicities of distant atoms and three-atom configurations. For example, multiplicities of the three-atom configurations depend in a nontrivial way on the density of defects.

A very simple model taking into account atomic defects is easily produced by using an iterative procedure acting on a perfect bcc lattice. The procedure begins with a central atom for which the first neighbors are chosen randomly with a fixed probability. Connectivity is ensured by imposing a minimum number of first neighbors. The procedure is repeated on the new atoms generated at the previous step. A maximum distance from the center is allowed, limiting the actual cluster size. The total number of atoms to be inserted is fixed ac-

cording to a selected density. This procedure allows one to build a highly connected network in the presence of a large number of atomic defects which greatly increase the surface-to-volume ratio. The final clusters have an approximate spherical shape with very irregular surfaces and the presence of voids and point defects. In Fig. 5 we show the calculated average multiplicities of the main two-atom and three-atom configurations present in models with a diameter of about 70 Å as a function of the relative atomic density. Parameters of the calculation were the generation probability p of the first neighbors (in this case $p=1/6$) and the minimum number N_m of neighbors allowed ($N_m=2$).

Obviously, the determination of a realistic model reproducing the atomic arrangement (and motion) in nanocrystalline materials including grain boundaries is beyond the scope of the present work. To this purpose, it would be certainly interesting to develop specific applications of molecular dynamics or other advanced computer simulation techniques in such systems showing large excess free volume. However, results presented here show that in presence of a low atomic density it is possible to obtain a locally ordered and connected network with very low average coordination numbers in agreement with EXAFS experimental data. In particular, according to Fig. 5(a), about 25% reduction of the first-neighbor CN is obtained with a 0.9 relative density. The reduction increases up to about 45% decreasing the relative density down to 0.5. The three-atom multiplicities are strongly damped as expected (from 45% up to about 65% for a 0.5 relative density). These numbers are of the same order as those found in the present work and in previous studies of nanocrystalline materials. Below a critical density (about 0.5 in this case) there is a slope change in the curves of Fig. 5, due to the combined action of both the probability of generation of neighbors and of the con-

dition of a minimum number of first neighbors. Below this critical density the reduction of neighbors tends to saturate.

Despite of its simplicity, this model is useful not only for demonstrating the possibility of a reduction of the CN's without complete loss of short-range order, but also to determine possible multiplicities of distant atoms and triangular configurations to be used to fit experimental EXAFS spectra of the nanocrystalline material under consideration. This last issue will be discussed in the next section.

D. *Ab initio* EXAFS data analysis of nanocrystalline iron

In this section the structural results of the *ab initio* MS data analysis of the EXAFS spectra of nanocrystalline iron are presented. Data analysis has been performed using the same criteria described in the case of crystalline iron (Sec. III B). In order to achieve a reasonable agreement between calculated and experimental data it is necessary to allow variations of the multiplicities of the two-atom and three-atom signals typical of the local bcc structure. Of course, a variation of the first-neighbor CN implies a reduction of the multiplicities of all the local two-atom and three-atom configurations. This topic has been discussed in detail in the previous section.

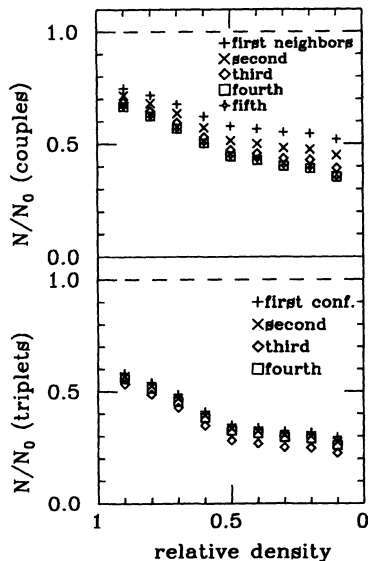In Fig. 6 the best-fit calculated $k^2\chi(k)$ signals are

FIG. 5. Multiplicities of two-atom (upper panel) and three-atom (lower panel) configurations derived from a bcc model (diameter of about 70 Å) which includes lattice vacancies. Results are presented as a function of the relative density ρ/ρ_0 (where ρ_0 is the density of the bulk).
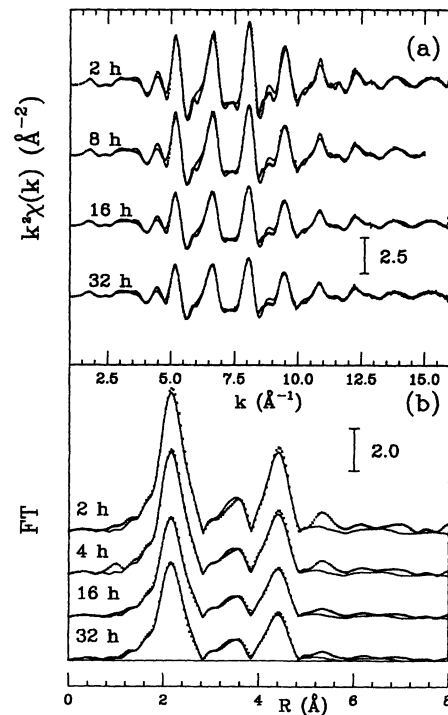

FIG. 6. Upper panel (a): comparison between experimental $k^2\chi(k)$ spectra of nanocrystalline iron prepared at different milling time (2 h, 8 h, 16 h, and 32 h) and the best-fit calculated signals obtained using multiple-scattering contributions. Lower panel (b): Fourier transform (FT) of the $k^2\chi(k)$ experimental spectra shown in the upper panel.

compared with the experimental EXAFS spectra of the nanocrystallites under consideration. Best-fit signals have been obtained allowing us to vary the multiplicities of the two-atom and three-atom configurations with respect to the crystalline case. The average first-neighbor coordination number N_1 has been allowed to move until convergence to a minimum was achieved. The multiplicities of the other two-atom and three-atom configurations were allowed to vary only in a restricted region of values, physically consistent with the observed degeneracy of the first neighbors. In particular, as the N_1 value has been found to be compatible with samples with a high defect density, multiplicity values obtained from Fig. 5 have been then used as a guideline.

The final best-fit values of the multiplicities of the main two-atom and three-atom configurations are reported in Fig. 7. Values obtained for the first three triangular configurations are characterized by a very high statistical error and are not shown. Values reported in Fig. 7 are in qualitative agreement with the results derived for the model described in the Sec. III C (Fig. 5). As expected, the defect density increases as a function of the milling time. Loss of coordination saturates after 16 h of mechanical working. The similarity between the 16 h and 32 h samples is confirmed also by looking at lattice strains as measured by x-ray diffraction.[13] In the case of the 16 h and 32 h samples the values of the multiplicities are compatible with high defect densities (corresponding to the region around 0.5 of relative density in Fig. 5).

The other structural parameters, such as the cell side, bond, angle variances, and correlations, were found to

be, for all the nanocrystalline samples, identical within the errors to those found in the case of crystalline iron. In particular we did not find any significant variation both in the average interatomic distances [a=2.854(5) Å] and in the first-neighbor bond variance $\sigma_R^2 = 4.5(6)$. The introduction of an asymmetric first-neighbor distribution was not found to improve significantly the fit although the β value was found to be slightly larger than in the crystalline case, $\beta = 0.2(1)$.

The results on the coordination numbers presented in Fig. 7 have been put to a test by calculating best-fit signals derived using different models for the multiplicities of the two-atom and three-atom signals. In particular, two different models have been considered. The first (A) consists in applying a uniform reduction factor to the multiplicities of the γ signals ($N = N_1$). This model is consistent with the assumption of the existence of a fraction x of atoms showing a perfect bcc local coordination plus a fraction $(1 - x)$ of atoms with a completely disordered structure. A second model (B) can be realized by applying exactly the relationships between the first-neighbor CN and the other multiplicities shown in Fig. 4. This schematization corresponds to consider the nanocrystallites as a collection of very small clusters (say, with diameter around 10 Å).

In Fig. 8 the FT spectra of the best-fit $\chi(k)$ signals, derived using the two models A and B, are compared with
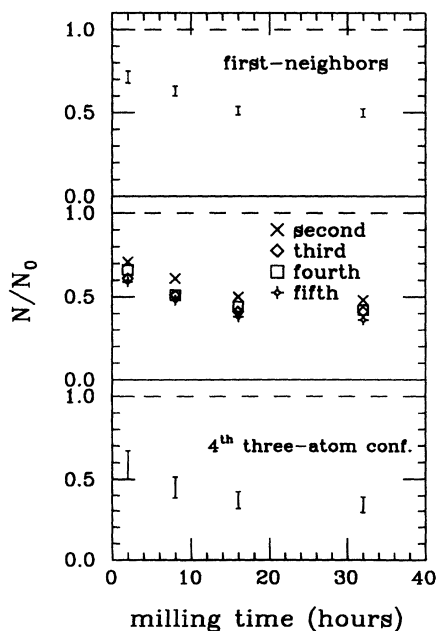

FIG. 7. First-neighbor coordination number as a function of milling time (a). In the middle panel (b) the best-fit values of the next four coordination shells are shown (error bar is about 15% of the values). The multiplicities of the fourth three-atom collinear configuration are shown in the lower panel. A good agreement with a model taking into account defects in the structure is found (see Fig. 5).
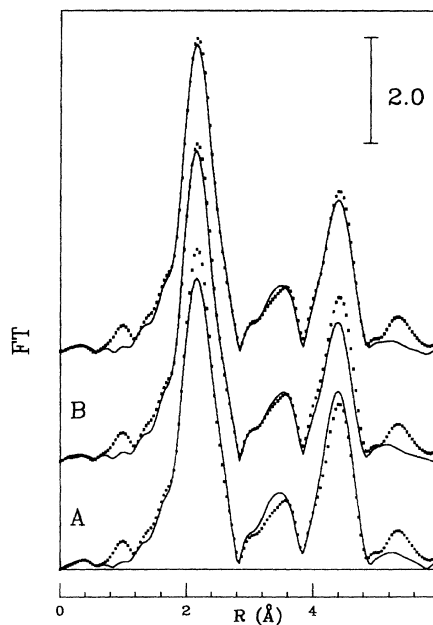

FIG. 8. Comparison between different best-fit Fourier transform (FT) spectra (8 h milling time) obtained using the same coordination number for all the two-atom and three-atom configurations (A); multiplicities derived from clusters of appropriate size (about 10 Å) in order to account for the reduction of the first-neighbor coordination number (B). The upper curve is the best-fit curve obtained using the coordination numbers of Fig. 7. The FT of the 8 h experimental spectrum is shown as dots in each case. Models A and B which do not properly account for lattice defects are not in agreement with the experimental spectrum.

the experimental signal (dots) of the 8 h milled sample and with the best-fit signal reported in Fig. 6. Both best-fit signals obtained using models A and B show an unacceptable worse agreement with the experimental signal as indicated by the higher values (of about a factor of 2) of the least-squares residual used to minimize the difference between experimental and calculated spectra. This is clearly seen in the FT spectra of Fig. 8 where the intensity of the peaks below 5 Å cannot be reproduced using the above-mentioned models. In particular, model A (lower curve) is not able to reproduce the relative intensity of the peaks. The weight of the third peak around 4.5 Å (and to a lesser extent of the second one at about 3.5 Å) is always too big in the simulated spectrum, and this effect cannot be reproduced by introducing a higher level of disorder of interatomic distances and angles (in this case we found $N \approx 0.65$ and $\sigma_R \approx 5 \times 10^{-3}$ Å^2). This is direct evidence of the importance of taking proper account of the increased reduction factor acting on the multiplicities of the distant atoms and particularly that of the fourth three-body collinear configuration. By using model B, instead, a nicer agreement is found (center curve). However, also in this case the intensity ratio between the first and the third FT peaks is wrong, indicating that multiplicities of distant atoms and triangular configurations are not correctly reproduced.

As a final remark we would like to point out that the very reduced multiplicities associated with two-atom and three-atom configurations involving distant atoms are also revealed by looking at the $\chi(k)$ experimental spectra where there is a detectable lack of high frequencies (see arrows in Fig. 1). Unfortunately, quantitative analysis of these very high-frequency weak features would implicate the use of many γ signals in the model probably including four-atom contributions.

E. XAS study of nanocrystalline iron at high temperature

In a final study, we have performed an *in situ* high-temperature annealing of the 32 h sample while recording x-ray-absorption spectra. We used an oven of novel design,[25] working in vacuum and capable of reaching very high temperatures in a few seconds. In Fig. 9 we present some of the near-edge absorption spectra which have been recorded as a function of temperature. For temperatures less than 910 °C the well-known Debye-Waller-like reduction of amplitudes of the near-edge structures is observed. At about 915±5 °C we have clearly observed the phase transition from α iron (bcc structure) to γ iron (fcc structure) which is characteristic of bulk crystalline iron ($T_m \approx 910$ °C). One typical near-edge XAS spectrum just above T_m is presented in Fig. 9 (upper curve). The different near-edge features related to the fcc local structure are clearly observable. This is the first direct observation that such nanocrystalline material undergoes the same structural transition of the bulk crystalline counterpart.

The 32 h sample has been heated up to about 1100 °C for about half an hour and then cooled down to room temperature. The total duration of the thermal
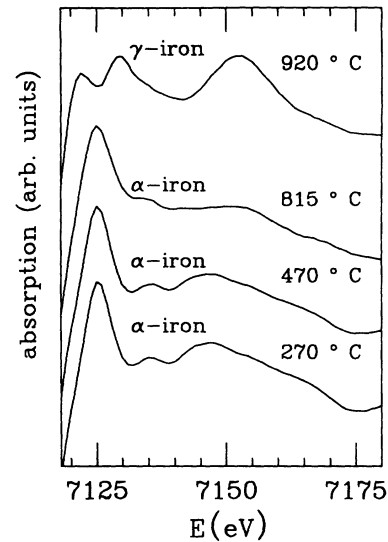

FIG. 9. Near-edge x-ray-absorption spectra of the Fe 32 h milled nanocrystalline sample at different temperatures. The transition between a bcc local structure (α) and a fcc one (γ) is evident.

treatment was about 120 min. In Fig. 10 the $k^2\chi(k)$ EXAFS spectra of the 32 h sample before (upper curve) and after (lower curve) annealing are presented [panel (a)]. Both experimental spectra (dots) and calculated signals (solid curves) are reported. In the lower panel (b)
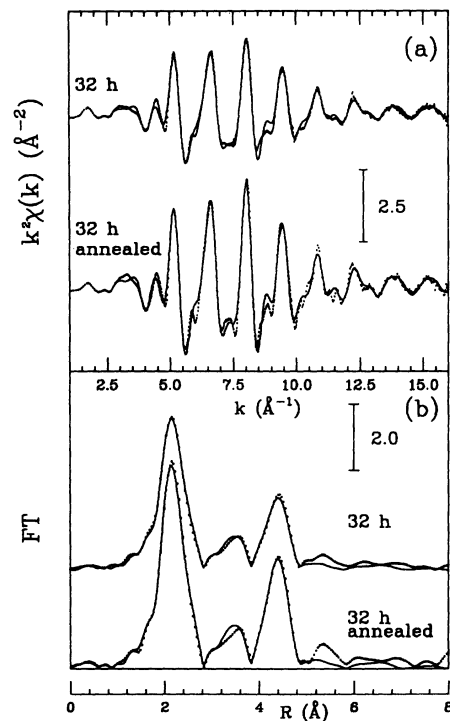

FIG. 10. Upper panel (a): comparison between experimental $k^2\chi(k)$ spectra (dots) of the 32 h nanocrystalline iron sample before and after annealing. The best-fit calculated signals obtained using multiple-scattering contributions are shown as solid curves. Lower panel (b): Fourier transform (FT) of the $k^2\chi(k)$ reported in the upper panel.

the FT spectra are also shown. The experimental spectra clearly show an increase of the amplitude of the $\chi(k)$ signal. An increase of the weight of the high-frequency components is also evident. The simple explanation for this phenomenon is the reduction of the density of defects obtained by high-temperature thermal treatment. This has to be expected because a lower density of defects is energetically favored. Moreover, it is well known that the average grain size rapidly increases as a function of temperature and the grain-boundary region, where the density of defects could be higher, tends to collapse (grain growth).

The EXAFS spectra show unambiguously that a high-temperature treatment reduces the density of the defects and provides a quantitative evaluation of the increase in local coordination. In the case of the 32 h annealed sample local coordination has been increased by about 35%. The first-neighbor CN has been found to be 0.67(4) of the bulk crystalline value, similarly to the cases of the 2 h and 8 h milled samples (see Fig. 7). Therefore, the results of the fitting procedure show that a quite high density of defects still persists. The other CN's and multiplicities are similar, as expected, to those found in the 2 h and 8 h cases.

IV. CONCLUSIONS

In this paper we have presented a multiple-scattering EXAFS data analysis of nanocrystalline iron prepared by high-energy ball milling. EXAFS spectra of nanocrystalline samples show a reduction of the amplitude which is a function of the milling time.

Quantitative structural results have been obtained by using a recently developed ab initio data-analysis method based on an expansion of the absorption cross section in terms of two-atom and three-atom MS contributions. The EXAFS spectrum of crystalline iron has been accurately analyzed by using such MS contributions obtaining

reliable values for interatomic distances and thermal disorder parameters. The amplitude reduction observed in the EXAFS spectra of nanocrystalline samples has been interpreted as due to the existence of a large density of structural defects, in agreement with previous observations by x-ray diffraction. A simple model taking into account only the existence of lattice vacancies has been described. The possibility of the observation of very low average coordination numbers is discussed and the characteristic enhanced reduction factors for three-atom multiple-scattering signals have been evaluated. EXAFS data analysis has confirmed the different reduction factors for the multiplicities of two-atom and three-atom signals in good agreement with the model obtained using a high density of defects. Other simple models obtained neglecting lattice defects have been shown to be unable to explain differences in the amplitude of the different frequency components of the experimental spectra.

EXAFS data recorded at high temperatures have shown the existence of the characteristic phase transition from α iron to γ iron in such nanocrystalline materials. Quantitative study of an annealed nanocrystalline sample has shown an increased first-neighbor coordination number in agreement with a reduction of the defect density.

The results presented in this paper provide deep insight into the local structure of mechanically produced nanocrystalline iron and strongly support the interpretation of the decrease of the local coordination as due to the existence of a large defect density in these materials. In particular, the use of multiple-scattering analysis probing three-particle correlations allowed us to increase the sensitivity to lattice defects in local structure. Generally speaking, the sensitivity of the EXAFS spectra to short-range local coordination and to the multiplicity of triangular configurations can be used to select between possible local structural models in nanocrystalline materials and clusters.

[1] H. Gleiter, Prog. Mater. Sci. **33**, 233 (1989).

[2] R. W. Siegel and G. J. Thomas, Ultramicroscopy **40**, 376 (1992).

[3] X-ray Absorption: Principles, Applications, Techniques of EXAFS, SEXAFS and XANES, edited by D. C. Koningsberger and R. Prins (Wiley, New York, 1988).

[4] A. Filipponi, A. Di Cicco, T. A. Tyson, and C. R. Natoli, Solid State Commun. **78**, 265 (1991).

[5] A. Filipponi and A. Di Cicco, Synchrotron Radiat. News **6**, 21 (1993).

[6] A. Filipponi, A. Di Cicco, M. Benfatto, and C. R. Natoli, Europhys. Lett. **13**, 319 (1990).

[7] A. Di Cicco and A. Filipponi, J. Non-Cryst. Solids **156-158**, 102 (1993); Europhys. Lett. **27**, 407 (1994).

[8] T. A. Tyson, K. O. Hodgson, C. R. Natoli, and M. Benfatto, Phys. Rev. B **46**, 5997 (1992).

[9] A. Di Cicco, S. Stizza, A. Filipponi, F. Boscherini, and S. Mobilio, J. Phys. B **25**, 2309 (1992).

[10] P. D'Angelo, A. Di Cicco, A. Filipponi, and N. V. Pavel, Phys. Rev. A **47**, 2055 (1993).

[11] A. Di Cicco and A. Berrettoni, Phys. Lett. A **176**, 375 (1993).

[12] E. Bonetti, G. Scipione, G. Valdré, G. Cocco, R. Frattini, and P. P. Macrì, J. Appl. Phys. **74**, 2053 (1993).

[13] E. Bonetti, G. Scipione, G. Valdré, S. Enzo, R. Frattini, and P. P. Macrì (unpublished).

[14] T. Haubold, R. Birringer, B. Lengeler, and H. Gleiter, Phys. Lett. A **135**, 461 (1989).

[15] M. Jaouen, P. Bouillard, T. Girardeau, P. Chartier, J. Mimault, and G. Tourillon, J. Phys. Condens. Matter **2**, 8113 (1990).

[16] T. Haubold, F. Boscherini, S. Pascarelli, S. Mobilio, and H. Gleiter, Philos. Mag. A **66**, 591 (1992).

[17] A. Balerna, E. Bernieri, P. Picozzi, A. Reale, S. Santucci, E. Burattini, and S. Mobilio, Phys. Rev. B **31**, 5058 (1985).

[18] B. S. Clausen, L. Gråbæk, H. Topsœ, L. B. Hansen, P. Stoltze, J. K. Nørskov, and O. H. Nielsen, J. Catal. **141**, 368 (1993).

[19] S. Enzo, E. Bonetti, I. Soletta, and G. Cocco, J. Phys. D **24**, 209 (1991).

[20] H. J. Fecht, E. Hellstern, Z. Fu, and W. L. Johnson, Met. Trans. A **21**, 2333 (1990).

[21] S. Enzo, G. Cocco, and P. P. Macrí, Key Eng. Mater. **49**, 81 (1993).

[22] E. Hellstern, H. J. Fecht, Z. Fu, and W. L. Johnson, J. Appl. Phys. **65**, 585 (1989).

[23] M. S. Boldrick, E. Yang, and C. N. J. Wagner, J. Non-Cryst. Solids **150**, 478 (1992).

[24] C. N. J. Wagner, E. Yang, and M. S. Boldrick, Adv. X-ray Anal. **35**, 585 (1992).

[25] A. Filipponi and A. Di Cicco, J. Nucl. Instrum. Methods B **93**, 302 (1994).

[26] A. Di Cicco, M. Berrettoni, R. Tossici, R. Marassi, and A. Filipponi, in *Proceedings of the Ninth International Symposium on Molten Salts*, edited by C. L. Hussey, D. S. Newman, G. Mamantov, and Y. Ito, The Electrochemical Society Proc. No. 94-13, (The Electrochemical Society, New York, 1994), p. 77.

[27] A. Filipponi, A. Di Cicco, and C. R. Natoli, in *Disordered Materials (Structure and Properties)*, Proceedings of the International Conference INDIAS-91, edited by S. K. Srivastava (INDIAS Publications, Indore, India, 1993); A. Filipponi, A. Di Cicco, and C. R. Natoli (unpublished).

[28] A. Filipponi, L. Ottaviano, M. Passacantando, P. Picozzi, and S. Santucci, Phys. Rev. E **48**, 4575 (1993).

[29] E. Nordlander, S. C. Lee, W. Cen, Z. Y. Wu, C. R. Natoli, A. Di Cicco, A. Filipponi, B. Hedman, K. O. Hodgson, and R. H. Holm, J. Am. Chem. Soc. **115**, 5549 (1993); T. E. Westre, A. Di Cicco, A. Filipponi, C. R. Natoli, B. Hedman, E. I. Solomon, and K. O. Hodgson, *ibid.* **116**, 6757 (1994).

[30] A. Filipponi, J. Phys. Condens. Matter **3**, 6489 (1991).

[31] W. L. Schaich, Phys. Rev. B **29**, 6513 (1984).

[32] A. Di Cicco, N. V. Pavel, and A. Bianconi, Solid State Commun. **61**, 635 (1987); A. Bianconi, A. Di Cicco, N. V. Pavel, M. Benfatto, A. Marcelli, C. R. Natoli, P. Pianetta, and J. Woicik, Phys. Rev. B **36**, 6426 (1987).

[33] M. Benfatto, C. R. Natoli, and A. Filipponi, Phys. Rev. B **40**, 9626 (1989).

[34] A. Filipponi, L. Lozzi, M. Passacantando, P. Picozzi, S. Santucci, and M. Diociaiuti, Phys. Rev. B **47**, 8494 (1993).

[35] By inserting only the cell side as a "global" geometrical parameter we implicitly assume that mean distances and angles coincide with that of the model bcc structure. This is not necessarily true, because EXAFS probes correlated distances and angles and therefore slight deviations of these quantities could be observed, depending on the local vibrational modes. However, the present assumption greatly reduces the independent fitting parameters and has been preferred although leading to a slight worse agreement between calculated and experimental data.

[36] B. K. Teo, J. Am. Chem. Soc. **103**, 3990 (1981).

[37] N. Motta, M. De Crescenzi, and A. Balzarotti, Phys. Rev. B **27**, 4712 (1983).

[38] E. Sevillano, H. Meuth, and J. J. Rehr, Phys. Rev. B **20**, 4908 (1979).

[39] A. Filipponi, A. Di Cicco, R. Zanoni, M. Bellatreccia, V. Sessa, C. Dossi, and R. Psaro, Chem. Phys. Lett. **184**, 485 (1991).

[40] S.-H. Chou, J. J. Rehr, E. A. Stern, and E. R. Davidson, Phys. Rev. B **35**, 2604 (1987).

[41] E. Burattini, P. D' Angelo, A. Di Cicco, A. Filipponi, and N. V. Pavel, J. Phys. Chem. **97**, 5486 (1993).

[42] G. Li, F. Bridges, and G. S. Brown, Phys. Rev. Lett. **68**, 1609 (1992).

[43] A. I. Frenkel, E. A. Stern, M. Qian, and M. Newville, Phys. Rev. B **48**, 12449 (1993).

[44] X. Zhu, R. Birringer, U. Herr, and H. Gleiter, Phys. Rev. B **35**, 9085 (1987).

[45] Z. S. Basinski, W. Hume-Rothery, and A. L. Sutton, Proc. R. Soc. London A **229**, 459 (1955).

[46] V. J. Minkiewicz, G. Shirane, and R. Nathans, Phys. Rev. **162**, 528 (1967).